Analysis of Fluorescent Proteins with a Nanoparticle Probe

Francisco A. Fernandez-Lima,*[,†] Michael J. Eller,[†] J. Daniel DeBord,[†] Michaella J. Levy,[†] Stanislav V. Verkhoturov,[†] Serge Della-Negra,[‡] and Emile A. Schweikert[†]

[†]Department of Chemistry, Texas A&M University, College Station, Texas 77843-3255, United States
[‡]Institut de Physique Nucléaire d'Orsay, 91406 Orsay, France

S *Supporting Information*

ABSTRACT: This Letter presents the first application of high-energy, single nanoparticle probes (e.g., 520 keV Au_{400} 2 nm NP) in the characterization of surfaces containing fluorescent proteins (e.g., GFP variants) by their coemitted photon, electron and secondary ion signals. NP-induced protein luminescence increases with the NP incident energy, is originated by the NP impact, and is transferred to the protein fluorophor via electronic energy transfer. Multielectron emission is observed per single NP impacts, and their distributions are specific to the target morphology and composition. Fragment ions of protein subunits consisting of 2−7 amino acid peptides are observed under individual NP impacts that can be correlated to the random protein orientation relative to the impact site (e.g., outer layer or "skin" of the protein).
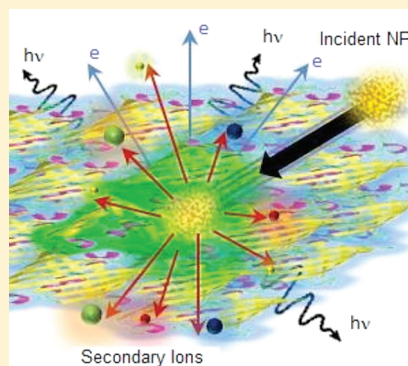
SECTION: Surfaces, Interfaces, Catalysis

We have recently reported that under single nanoparticle impacts (e.g., C_{60} and Au_{400} NPs) it is possible to detect the coemission of photons, electrons, and secondary ions on the nanometer level.[1,2] In particular, ion-induced photon emission from single projectile impacts can be observed from model fluorophores (e.g., sulforodhamine and fluorescein isothiocyanate).[1] The use of fluorescent tags to give a visual readout on a protein in biological analysis has become common practice over the last decades. In particular, one variant of protein tagging has been developed based on the green fluorescent protein (GFP) from the jellyfish *Aequoria Victoria*[3] and its different colored variants (e.g., YFP, BFP, and RFP).[4] Their most relevant feature is the ease with which they may be assembled and introduced into the cytoplasm and that their fluorescence is due to an internal interaction between amino acids within the protein. These studies are normally based on the localization of the fluorescent tag using optical microscopy techniques,[5,6] but they do not provide information on the chemical environment of the protein. In the present Letter, we present the first experimental observation of photon emission when fluorescent proteins are bombarded with individual nm-size projectiles. In particular, photon emission is correlated with the emission of electrons and analyte-specific secondary ions (SIs) from a nanometric volume ($\sim 10^3$ nm^3).

An experimental setup that comprises a gold cluster ion source, an electron emission microscope, a photon detector, and a time-of-flight (ToF) mass spectrometer were used for this study.[7,8] The gold cluster primary ion beam consists of a Au-liquid metal ion source (Au-LMIS) coupled to a 100 kV Pegase platform.[9] The Au-LMIS is floated to 20 kV relative to the Pegase platform and can produce a variety of projectiles,

ranging from atomic $Au_1^{+1,2}$ to polyatomic Au_{2-9}^{+1} to massive Au_{100n}^{+n} clusters; more details on the primary ion distribution produced by the Au-LMIS can be found in ref 10. The NP projectile used in this study was Au_{400}^{+4}, which is $\sim$2 nm in diameter. Co-emitted photons, electrons and secondary ions were collected per projectile impact analogously to the method used in refs 1 and 2. In brief, photons were detected using a photo multiplier (PMT, R4220P model from Hamamatsu Photonics) with an active window from 185 to 710 nm and a maximum detection efficiency of 22% at 410 nm, which was positioned behind the target (solid angle of 0.6 π sr). Details of the electron emission microscope can be found elsewhere.[11] In brief, electrons emitted from the impact site were accelerated to 10 keV and then deflected using a weak magnetic field toward an electron emission microscope where the initial signal was amplified and later detected using a position sensitive detector. The electron signal was used as a ToF start signal, and the electron images obtained from the position sensitive detector were processed to determine the number of electrons emitted per impact using in-house software.[12] Secondary ions were accelerated to 10 keV and analyzed using an in-house built ToF analyzer ($\sim$1.7 m long) equipped with a two-stage electrostatic mirror. ToF signals of the SIs were collected using a multianode, microchannel plate-based detector and were stored in a multichannel time-to-digital converter (CTNM4 TDC, IPN, Orsay). A typical acquisition consists of 500k to 2M
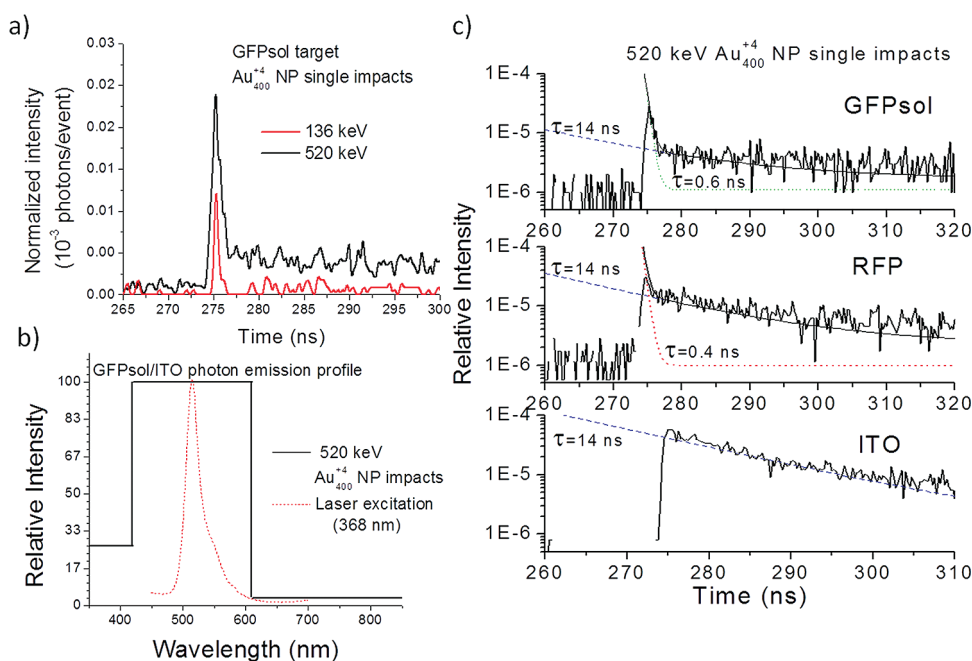
Figure 1. (a) Time-resolved photon spectra from GFPsol impacted by individual 136 and 520 keV Au$_{400}$ NPs, (b) photon emission profile of the GFPsol surface under NP impact and under laser excitation (368 nm), and (c) time-resolved photon spectra of GPPsol, RFP, and ITO surfaces under single NP impacts. Notice the two exponential decays for the GFPsol and RFP cases.

individual impacts. The photon signals from individual impacts were time delayed and stored in one of the TDC channels. Spectroscopic features of the photon emission were studied using optical filters from Oriel (Stratford, CT), with near 100% transmission in the 435−2800 and 610−2800 nm wavelength range.

A description of the fluorescent protein purification protocol can be found elsewhere.[13] GFPsol and RFP proteins were expressed recombinantly in *Escherichia coli* BL21(DE3) competent cells. After expression for 16 h at 24 °C, cells were disrupted by sonication. The soluble protein was purified by ammonium sulfate cuts, anion exchange, and size exclusion chromatography.[14] In particular, GFPsol has mutations at: F64L S65T F99S M153T V163A (GFPsol and RFP protein sequences can be found in the Supporting Information). It should be noted that the GFPsol and RFP chromophores form without the addition of an external stimulus or cofactor. Protein samples were dissolved in 50% water/methanol and electrosprayed to guarantee good surface coverage and homogeneity. All samples were deposited onto a 70−100 Ω/sq indium tin-oxide-coated glass (ITO/glass) substrate from Sigma Aldrich (St. Louis, MO). Photon absorption and fluorescence emission experiments confirmed the integrity of the chromophores after deposition onto the ITO/glass substrates.

Photon emission was studied as temporally and spatially discrete events; that is, time-resolved photon spectra were collected using individual NP impacts. As the NP projectile energy increases, an increase in the photon emission yield is observed. (See Figure 1a.) This photon emission increase is directly associated with the amount of energy deposited during the impact. That is, during the NP hydrodynamic penetration, the larger the incident kinetic energy the larger the energy deposited at the impact site. The spectroscopic properties of the photon emission from NP impacts on GFPsol were studied using transmission filters and are summarized in Figure 1b. Upon NP impact, photon emission from GFPsol is primarily in

the 435−610 nm wavelength interval, which corresponds to the GFPsol emission band observed by laser-induced fluorescence from the same target (Figure 1b). Figure 1c contains time-resolved spectra for GFPsol, RFP, and ITO samples from individual NP impacts (520 keV Au$_{400}$ 2 nm NP). Inspection of Figure 1c shows that the ITO time-resolved photon emission profile has a single exponential decay form ($\tau = 14 \pm 1$ ns). However, the GFPsol and RFP time-resolved photon spectra have a two-component, exponential decay profile: a fast component with $\tau = 0.6 \pm 0.1$ and 0.4 ± 0.1 ns, respectively, and the same slow component $\tau = 14 \pm 1$ ns. We interpret the two component decay profile as electronic energy transfer from the NP excitation during the NP impact (broad band emission at 300−600 nm[15]) to the GFPsol and RFP fluorescent proteins. The ITO photon emission can be attributed to the gold NP projectile luminescence because similar fluorescence decay times have been observed from laser excitation of individual gold NPs.[15,16] For example, the decay time of gold cluster luminescence is related to the cluster size,[17,18] and in the case of nanometer-size clusters could be from a few to tens of nanoseconds (Au$_{400}$ NP is ∼2 nm in size). It should be noted that during the NP penetration, the NP size may decrease due to near track friction related processes (∼20 nm range and ∼1 ps penetration time for 520 keV Au$_{400}$$^{+4}$ NP impacts). Although the electronic excitation/transfer mechanism remains to be elucidated, the experimental data suggest that the energy deposited by the NP projectile is sufficient to induce electronic excitation without fragmenting the α-helix subunits that contain the chromophores in the GFPsol and RFP proteins. This scenario is more likely to occur if: (i) emission comes from protein molecules located near the NP impact site or (ii) the NP projectile grazes the protein rather than striking it directly. Differences in the fluorescence decay times of GFPsol and RFP fast components may be related to the electronic energy transfer to the protein chromophores, which in some cases may also involve homo-FRET processes; that is, homo-FRET can
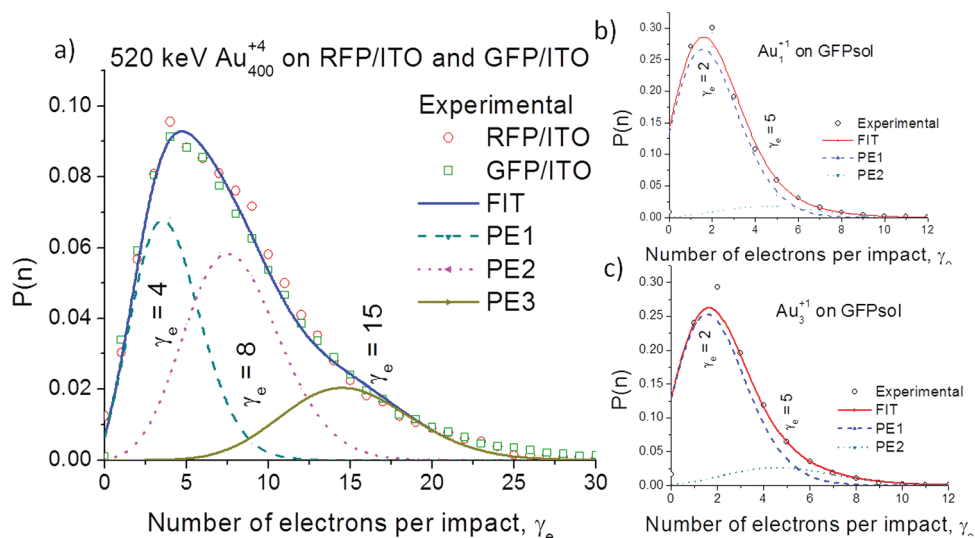
Figure 2. (a) 520 keV Au_{400} NP induced electron emission distributions for the GFPsol and RFP surfaces. (b,c) Single impact 130 keV Au_1- and Au_3-induced electron emission distributions for the GFPsol surface. Notice that electron distributions follow a two to three component Poisson distribution.
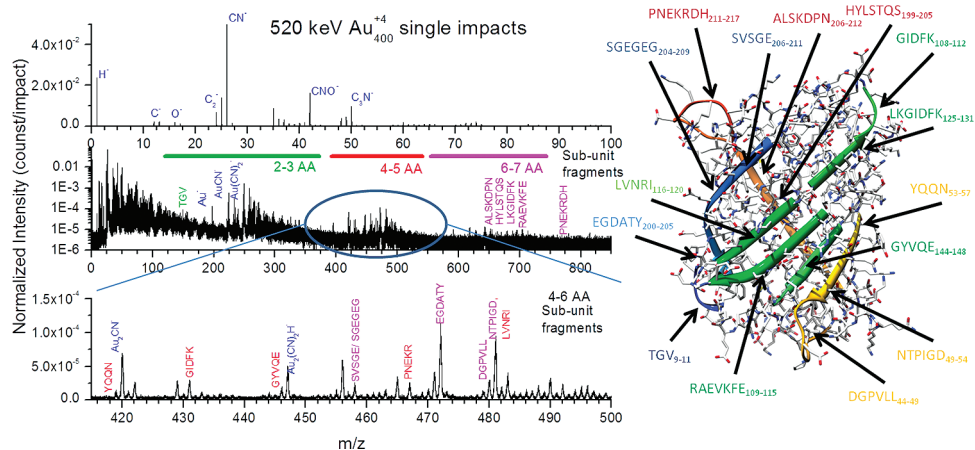
Figure 3. (Left) Typical secondary ion spectrum of GFPsol bombarded with individual 520 keV Au_{400} NP projectiles. Notice the emission of 2−7 AA peptide subunits. (Right) Location of the peptide subunits identified from the MS spectra in the GFPsol secondary structure model;[28] backbone structures of the identified peptide subunits are represented by ribbons. Notice that the peptide subunit MS signals come from the outer layer ("skin") of the GFPsol molecule.

occur between similar chromophores without changes in either fluorescence steady-state intensity or the fluorescence lifetime. GFP mutants have been shown to have different fluorescent lifetimes (on the order of few nanoseconds);[19] however, no changes in the decay time have been observed with different solvent conditions.[20] Photon emission was also observed with individual 130 keV Au projectiles with lower emission yield relative to the 520 keV Au_{400} NP projectiles (∼10 fold). In the case of Au projectiles, the photon emission showed a single component exponential decay with a few nanosecond lifetime. A more detailed study of the photon emission from protein surfaces for the case of polyatomic projectiles (e.g., Au_1–Au_9) will be described in a future paper.

Coincidental electron emission was studied per projectile impact. As a general trend, multielectron emission was observed from the GFPsol and RFP surfaces. (See Figure 2.) The GFPsol and RFP surfaces showed similar NP-induced electron emission distributions. The electron distributions can be described as Poisson distributions (PE1, PE2, and PE3) with mean values of

γ_e = 4, 8, and 15. Electron distributions from atomic ion bombardment have also shown a Poisson-like distribution,[21,22] which have been attributed to the stochastic nature of the particle emission during ion bombardment.[23]

For example, in the case of Au_1 and Au_3 projectile impacts, GFPsol electron distributions follow a Poisson distribution (PE1 and PE2) with mean values of γ_e = 2 and 5 (Figure 2). Recent experiments using individual C_{60} impacts have shown mainly one or two PE distributions over a wide variety of targets, where the mean value of the distribution varies as a function of target composition and morphology.[2,11,24] In the case of NP projectiles, the electron emission is observed where kinetic electron emission from comparable velocity atomic projectiles does not occur.[25,26] Moreover, because of the low charge state of the gold NPs (+1 to +4), the phenomenon cannot be attributed to a potential electron emission mechanism. That is, the unexpected multielectron emission observed under NP impacts is mainly attributed to the electronic excitation near the impact site. In the case of GFPsol

and RFP surfaces, the multicomponent electron distribution suggests that the projectile impact generates secondary energy-transfer mechanisms near the impact site (electronic excitation), which are related to the morphology of the adjacent molecular components, or proteins in our case. In particular, the electronic excitation near the impact site is responsible for coincidental electron and photon emission, which is characteristic of both target composition and morphology.

Abundant secondary ion emission is also observed from individual NP impacts on GFPsol and RFP surfaces, in contrast with atomic and small polyatomic projectile impacts. The secondary ion emission can be characterized by the observation of analyte-specific small fragments (e.g., CN^-, CNO^-) and larger protein subunit fragments. The small fragments ($m/z < 100$) are a common feature of ion-induced mass analysis and are fragmentation debris from molecules at the surface; their distribution and relative abundance vary with the projectile size and energy. That is, the small fragment secondary ion yield increases with the projectile size and energy. (See the Supporting Information for comparison among 260 keV Au_1^{+2}, 130 keV Au_1^{+1}, 130 keV Au_3^{+1}, 130 keV Au_9^{+1}, and 520 keV Au_{400}^{+4} secondary ion emission.) Protein subunit fragments are observed during NP impacts and can be correlated with the protein sequence. It should be noted that the protein subunit fragments follow a different formation mechanism from that observed during collision-induced dissociation or surface-induced dissociation experiments. In the case of NP impacts, the distribution of protein subunits containing 2−7 amino acid suggest that the peptide fragments were formed near the impact site and may relate to the protein orientation relative to the impact site (Figure 3). For example, most of the subunit fragment signals correspond to protein segments located on the outer shell of the proteins (β-barrel domain). That is, the outer shell or "skin" fragments are preferentially emitted during the NP impact, whereas subunit fragments from the inner core (α-helix domain) are not observed. The distribution of protein subunits suggests that backbone cleavage near the impact site promotes the formation of these protein-specific subunit fragment ions.

The results presented here suggest that discrete and temporally isolated NP impacts on surfaces containing fluorescent proteins can be used to probe the protein environment via the inspection of the coemitted photon, electron, and SI signals. Although the mechanism coupling the NP incident energy to the surface electronic excitation remains to be elucidated, the experimental results suggest that there is an electronic energy transfer between the NP probe and the protein chromophore. The enhancement in secondary ion emission under high-energy NP impacts produces abundant protein-specific subunit fragments (2−7 amino acid fragments) in addition to the characteristic low-mass fragment species. In particular, the characteristic photon, electron, and SI information can be used as surface fingerprints for the chemical environment of the fluorescent proteins. This approach can be further complemented by the generation of SI-specific surface maps by the localization of the impact site via the emitted electrons.[8,11,27]

ASSOCIATED CONTENT

Ⓢ Supporting Information

GFPsol and RFP protein sequence information, as well as GFPsol secondary ion spectra as a function of the projectile size (e.g., 260 keV Au_1^{+2}, 130 keV Au_1^{+1}, 130 keV Au_3^{+1}, 130 keV Au_9^{+1}, and 520 keV Au_{400}^{+4} NP). This material is available free of charge via the Internet at http://pubs.acs.org.

AUTHOR INFORMATION

Corresponding Author

*E-mail: ffernandez@chem.tamu.edu.

REFERENCES

(1) Fernandez-Lima, F. A.; Pinnick, V. T.; Della-Negra, S.; Schweikert, E. A. Photon Emission from Massive Projectile Impacts on Solids. *Surf. Interface Anal.* **2011**, *43*, 53−57.

(2) Fernandez-Lima, F. A.; Eller, M. J.; Verkhoturov, S. V.; Della-Negra, S.; Schweikert, E. A. Photon, Electron, and Secondary Ion Emission from Single C60 keV Impacts. *J. Phys. Chem. Lett.* **2010**, *1*, 3510−3513.

(3) Inouye, S.; Tsuji, F. I. Aequorea Green Fluorescent Protein: Expression of the Gene and Fluorescence Characteristics of the Recombinant Protein. *FEBS Lett.* **1994**, *341*, 277−280.

(4) Heim, R.; Tsien, R. Y. Engineering Green Fluorescent Protein for Improved Brightness, Longer Wavelengths and Fluorescence Resonance Energy Transfer. *Curr. Biol.* **1996**, *6*, 178−182.

(5) Lippincott-Schwartz, J.; Patterson, G. H. Development and Use of Fluorescent Protein Markers in Living Cells. *Science* **2003**, *300*, 87−91.

(6) Ellenberg, J.; Lippincott-Schwartz, J.; Presley, J. F. Dual-Colour Imaging with GFP Variants. *Trends Cell Biol.* **1999**, *9*, 52−56.

(7) Fernandez-Lima, F. A.; Post, J.; DeBord, J. D.; Eller, M. J.; Verkhoturov, S. V.; Della-Negra, S.; Woods, A. S.; Schweikert, E. A. Analysis of Native Biological Surfaces Using a 100 kV Massive Gold Cluster Source. *Anal. Chem.* **2011**, *83*, 8448−8453.

(8) Fernandez-Lima, F. A.; Eller, M. J.; DeBord, J. D.; Verkhoturov, S. V.; Della-Negra, S.; Schweikert, E. A. On the Surface Mapping using Individual Cluster Impacts. *Nucl. Instrum. Methods Phys. Res., Sect. B* **2011**, doi: 10.1016/j.nimb.2011.07.092.

(9) Della-Negra, S.; Arianer, J.; Depauw, J.; Verkhoturov, S. V.; Schweikert, E. A. The Pegase Project, A New Solid Surface Probe: Focused Massive Cluster Ion Beams. *Surf. Interface Anal.* **2011**, *43*, 66−69.

(10) Bouneau, S.; Della-Negra, S.; Depauw, J.; Jacquet, D.; Le Beyec, Y.; Mouffron, J. P.; Novikov, A.; Pautrat, M. Heavy Gold Cluster Beams Production and Identification. *Nucl. Instrum. Methods Phys. Res., Sect. B* **2004**, *225*, 579−589.

(11) Verkhoturov, S. V.; Eller, M. J.; Rickman, R. D.; Della-Negra, S.; Schweikert, E. A. Single Impacts of C60 on Solids: Emission of Electrons, Ions and Prospects for Surface Mapping. *J. Phys. Chem. C* **2009**, *114*, 5637−5644.

(12) Eller, M. J.; Verkhoturov, S. V.; Della-Negra, S.; Rickman, R. D.; Schweikert, E. A. Real-Time Localization of Single C60 Impacts with Correlated Secondary Ion Detection. *Surf. Interface Anal.* **2011**, *43*, 484−487.

(13) Deschamps, J. R.; Miller, C. E.; Ward, K. B. Rapid Purification of Recombinant Green Fluorescent Protein Using the Hydrophobic Properties of an HPLC Size-Exclusion Column. *Protein Expression Purif.* **1995**, *6*, 555−558.

(14) Barondeau, D. P.; Kassmann, C. J.; Tainer, J. A.; Getzoff, E. D. The Case of the Missing Ring: Radical Cleavage of a Carbon−Carbon

Bond and Implications for GFP Chromophore Biosynthesis. *J. Am. Chem. Soc.* **2007**, *129*, 3118−3126.

(15) Wilcoxon, J. P.; Martin, J. E.; Parsapour, F.; Wiedenman, B.; Kelley, D. F. Photoluminescence from Nanosize Gold Clusters. *J. Chem. Phys.* **1998**, *108*, 9137−9143.

(16) Dulkeith, E.; Niedereichholz, T.; Klar, T. A.; Feldmann, J.; von Plessen, G.; Gittins, D. I.; Mayya, K. S.; Caruso, F. Plasmon Emission in Photoexcited Gold Nanoparticles. *Phys. Rev. B* **2004**, *70*, 205424.

(17) Zheng, J.; Zhang, C.; Dickson, R. M. Highly Fluorescent, Water-Soluble, Size-Tunable Gold Quantum Dots. *Phys. Rev. Lett.* **2004**, *93*, 077402.

(18) Imura, K.; Nagahara, T.; Okamoto, H. Near-Field Two-Photon-Induced Photoluminescence from Single Gold Nanorods and Imaging of Plasmon Modes. *J. Phys. Chem. B* **2005**, *109*, 13214−13220.

(19) Scruggs, A. W.; Flores, C. L.; Wachter, R.; Woodbury, N. W. Development and Characterization of Green Fluorescent Protein Mutants with Altered Lifetimes. *Biochemistry* **2005**, *44*, 13377−13384.

(20) Suhling, K.; Davis, D. M.; Phillips, D. The Influence of Solvent Viscosity on the Fluorescence Decay and Time-Resolved Anisotropy of Green Fluorescent Protein. *J. Fluoresc.* **2002**, *12*, 91−95.

(21) Krebs, K. H. Secondary Electron Release at Metal Surfaces Due to Positive Molecular Ions. *Ann. Phys.* **1964**, *13*, 97−100.

(22) Winter, H. P.; Vana, M.; Lemell, C.; Aumayr, F. Interaction of Slow Multicharged Ions with Solid Surfaces: Current Concepts and New Information on Slow Electron Emission. *Nucl. Instrum. Methods Phys. Res., Sect. B* **1996**, *115*, 224−232.

(23) da Silveira, E. F.; Duarte, S. B.; Schweikert, E. A. Multiplicity Analysis: A Study of Secondary Particle Distribution and Correlation. *Surf. Sci.* **1998**, *408*, 28−42.

(24) Eller, M. J.; Verkhoturov, S. V.; Della-Negra, S.; Schweikert, E. A. Electron Emission from Hypervelocity C_{60} Impacts. *J. Phys. Chem. C* **2010**, *114*, 17191−17196.

(25) Brunelle, A.; Chaurand, P.; Della-Negra, S.; Beyec, Y. L.; Parilis, E. Secondary Electron Emission Yields from a CsI Surface Under Impacts of Large Molecules at Low Velocities (5×10^3−7×10^4 m/s). *Rapid Commun. Mass Spectrom.* **1997**, *11*, 353−362.

(26) Aumayr, F.; Betz, G.; Mark, T. D.; Scheier, P.; Winter, H. P. Electron Emission from a Clean Gold Surface Bombarded by Slow Multiply Charged Fullerenes. *Int. J. Mass Spectrom.* **1998**, *174*, 317−328.

(27) Eller, M. J.; Verkhoturov, S. V.; Fernandez-Lima, F. A.; DeBord, J. D.; Schweikert, E. A.; Della-Negra, S. Simultaneous Detection and Localization of Secondary Ions and Electrons from Single Massive Cluster Impacts. *Surf. Interface Anal.* **2012**, in press.

(28) Barondeau, D. P.; Putnam, C. D.; Kassmann, C. J.; Tainer, J. A.; Getzoff, E. D. Mechanism and Energetics of Green Fluorescent Protein Chromophore Synthesis Revealed by Trapped Intermediate Structures. *Proc. Natl. Acad. Sci. U.S.A.* **2003**, *100*, 12111−12116.

341

dx.doi.org/10.1021/jz201547x | *J. Phys. Chem.Lett.* 2012, 3, 337−341